TOWARDS METABOLIC MAPPING OF THE HUMAN RETINA

D. Schweitzer, S. Schenke, M. Hammer, F. Schweitzer, S. Jentsch
Experimental Ophthalmology, University of Jena, Bachstr. 18, D-07743 Germany

Eckhard Birckner
Physical Chemistry, University of Jena, Lessingstr. 10, D-07743 Germany

W. Becker, A. Bergmann
Becker & Hickl GmbH, Nahmitzer Damm 30, D-12277 Berlin, Germany

Correspondence to: Doz. Dr. D. Schweitzer
                      Eye Clinic, University of Jena,
                      Experimental Ophthalmology,
                      Bachstr. 18
                      07743 Jena
                      Germany
                      e-mail: Dietrich.schweitzer@med.uni-jena.de

ABSTRACT: We recorded fluorescence excitation spectra, fluorescence emission spectra, and fluorescence lifetime data for endogenous fluorophores expected at the fundus of the human eye. Effective spectra were calculated by multiplying these spectra by spectral transmission curves of the ocular medium. We found that the fluorescence of the fundus is dominated by Lipofuscin, FAD, AGE, and connective tissue. The excitation of NADH at the fundus appears unlikely. Based on the effective spectra of the fluorophores, we propose excitation and emission wavelength intervals optimised to separate the fluorescence signals of the fluorophores.
We used the results to optimise a fluorescence-lifetime imaging (FLIM) laser scanning ophthalmoscope. The device uses multi-dimensional time-correlated single-photon counting (TCSPC) to record lifetime images of the ocular fundus in two wavelength intervals simultaneously. FLIM images and reflection images are recorded simultaneously in short time intervals. Eye motion is corrected by deriving alignment vectors from the reflection images and applying them to the FLIM data.
The quality of the data is sufficient to apply a double- and triple-exponential fit to the decay data in the individual pixels. By comparing lifetime images obtained at different excitation wavelength and in different emission wavelength intervals the lifetime components could be attributed to different fluorophores and anatomical structures of the eye. The fastest lifetime component of typically 190 ps is related to lipofuscin in the retinal pigment epithelium, the second fastest of about 1 ns to the neural retina. The slowest component of about 5.5 ns is likely to originate in the connective tissue and the crystalline lens.

INTRODUCTION

In the last decades studies of metabolic function in the retina have been focused on micro-circulation, in particular on the blood flow (Cunha-Vaz and Lima, 1978; Oswald et al., 1983; Riva et al., 1972; Sato et al., 2006; Vilser et al., 1986) and the arterial oxygen saturation (Beach et al., 1999; Delori et al., 1981; Hickham et al., 1963; Laing et al., 1975; Schweitzer et al., 1999; Schweitzer et al., 1995). By combining these parameters the supply of the tissue with oxygen can be determined. Moreover, the arterio-venous difference of the oxygen saturation can be used as an indicator of the oxygen consumption in the tissue (Schweitzer et al., 1995). Unfortunately these approaches suffer from a serious limitation: The venous oxygen saturation increases both with the age and with the progress of a number of eye diseases, e.g. diabetic retinopathy. The tissue is then apparently oversupplied with oxygen. However, in fact the retinal tissue is hypoxic because the increased resistance in vessel walls of capillaries and of cell membranes hinders the diffusion of oxygen to the mitochondria.

Functional imaging of the retina should therefore focus on parameters that are specific of the metabolism in the cells. A suitable approach was first proposed by Chance (Chance, 1976). Differences in the partial pressure of oxygen can be determined by measuring variations in the autofluorescence of redox pairs of co-enzymes, in particular $NAD – NADH^+ + H^+$ (oxidised and reduced nicotinamidadenindinucleotide) and $FAD - FADH_2$ (oxidised and reduced flavinadenindinucleotide). These redox pairs act as electron carriers in oxidative phosphorylation in mitochondria. Autofluorescence measurements were found about 3 orders more sensitive to metabolic changes than measurements of the oxygen saturation (Chance, 1976).

Other endogenous fluorophores of interest are the ageing pigment, lipofuscin (Delori et al., 1995; Eldred and Katz, 1988; Feeney-Burns et al., 1980), advanced glycation end products, AGE (Ishibashi et al., 1998), collagen, and elastin. The detection and discrimination of these fluorophores might be a helpful tool to discover functional alterations by age-related macular degeneration, diabetic retinopathy or glaucoma. Lipofuscin has been found the dominating fluorophore in retinas with age-related macular degeneration, (Delori et al., 1995; Eldred and Katz, 1988; Feeney-Burns et al., 1980; Holz et al., 2001).
Lipofuscin is most efficiently excited at 380 nm. However, excitation wavelengths this short cannot be used in the eye because they are blocked by the absorption in the crystalline lens. Fortunately, the excitation spectrum of lipofuscin is relatively broad. Thus, even at a wavelength of 488 nm and an excitation power below the maximum permissible exposure (ANSI, 2000) laser scanning ophthalmoscopes are able to record reasonable images. The images were integrally detected between 520 nm and 700 nm (Bindewald et al., 2005; Einbock et al., 2005; von Rückmann et al., 1995; von Rückmann et al., 2002).

To apply autofluorescence as a diagnostic tool and for studying metabolic processes two requirements have to be fulfilled. First, minor fluorophores, emitting a very weak fluorescence must be separated from the covering strong fluorescence of lipofuscin. Second, the fluorophores must be discriminated with high lateral resolution in 2 - dimensional fundus images.

There are some serious limitations making autofluorescence detection at the human ocular fundus difficult. Of course, the exposure must be kept low enough to avoid any photodamage of the eye. Maximum permissible exposure values are given in (ANSI, 2000). The low excitation power

results in low fluorescence intensity and, consequently, long acquisition time. The accumulation of autofluorescence images therefore requires tracking and correction of the eye motion.

Moreover, there is fluorescence from all the parts of the eye in front of the fundus, especially from the crystalline lens. Detection of these unwanted signals has to be suppressed by using a scanning technique with confocal detection. However, the suppression is not perfect because the eye lens has a limited numerical aperture and considerable aberrations. Further improvement may be obtained by separation of apertures for illumination and observation (Schweitzer et al., 2005a).

In any case, excitation and detection of fundus fluorophores is limited to the ocular transmission window which extends from about 400 nm to 900 nm (Geeraets and Berry, 1968; Pokorny et al., 1987; van Norren and Vos, 1974). Even inside this window the apparent excitation and emission spectra are changed by variation in the absorption. Moreover, xanthophyll contained in the macula alters the fluorescence spectrum of the pigment epithelium (Delori et al., 2001). Efficient discrimination of fluorophores only by their excitation and emission spectra is therefore not feasible.

A considerable improvement can be expected from fluorescence lifetime detection. The fluorescence lifetime is not influenced by the wavelength-dependent transmission of the ocular media or by absorption of pigments in the neighbourhood of fluorophores (Qui et al., 2005). Moreover, lifetime detection adds an additional discrimination parameter to distinguish different fluorophores. Lifetime detection is even sensitive to intracellular parameters, because these change the fluorescence lifetime of the fluorophores.

It is often objected against fluorescence lifetime imaging that it requires a large number of photons to be detected and thus results in long acquisition times. This is, however, not generally correct. It has been shown that lifetime data can be obtained from a given number of detected photons with the same standard deviation as the fluorescence intensity (Gerritsen et al., 2002; Köllner and Wolfrum, 1992). It is only required that the fluorescence decay curves be recorded with an instrument response function much shorter than the fluorescence decay time, with negligible background, and over a time interval much longer than the decay time.

Fluorescence lifetime imaging (FLIM) based on multi-dimensional time-correlated single-photon counting (TCSPC) comes close to the ideal (Becker, 2005; Bird et al., 2005; Lakowicz, 1999; Schweitzer et al., 2004b; Schweitzer et al., 2000). Moreover, the techniques are capable of multi-wavelength detection, excitation wavelength multiplexing, and fast scanning. First time-resolved autofluorescence images of the human fundus were recorded by Schweitzer (Schweitzer et al., 2004a; Schweitzer et al., 2004b; Schweitzer et al., 2000).

In this article, excitation and emission spectra of endogenous fluorophores were investigated. Taking into account the limited transmission of the ocular media, effective excitation and emission spectra were derived. The results were used to optimise a time-resolved laser scanning ophthalmoscope (Schweitzer et al., 2004b). Typical lifetime images taken with the optimised setup are shown and discussed.

FLUORESCENCE PROPERTIES OF FLUOROPHORES EXPECTED IN THE FUNDUS

Excitation and emission spectra

The excitation and emission spectra were measured with the Fluorolog, Jobin Yvon Spex. The absorbance of the substances was adjusted to about 0.08. Fluorescence emission spectra were

recorded for excitation at 446 nm and 470 nm, according to the laser diodes used in the laser scanning ophthalmoscope.

Transmission curves of the ocular media were calculated by using data published by Pokorny (Pokorny et al., 1987). The transmission curves depend on the age of the person. The data presented below were calculated for a 20 years old person.

The most intensively emitting fluorophore at the fundus is Lipofuscin (Delori et al., 1995; Feeney-Burns et al., 1980). As shown by Eldred and Katz (Eldred and Katz, 1988), Lipofuscin is a mixture of at least 10 fluorophores. Until now, only the structure of component VIII (A2E) was determined as N-retinylidene-N-retinylethanolamine (Eldred and Lasky, 1993). A2E is a by-product of the visual cycle. It accumulates in the retinal pigment epithelium over the time of the life (Sparrow et al., 2003). For the experiments shown below A2E was synthesised according to Parish (Parish et al., 1998). Excitation and emission spectra were measured after adjusting the absorbance lower than 0.08 (A2E 12.8 µM, dissolved in ethanol).

Fig. 1 shows excitation and emission spectra of A2E, in comparison to the ocular transmission. A2E has a local excitation maximum at 437 nm when the emission is measured at 660 nm. This spectrum is in agreement with data of Sparrow (Sparrow et al., 2000). When A2E was excited at 446 nm, the emission maximum was found at 600 nm. A comparison of the excitation spectrum with the transmission of the ocular media shows that A2E in the fundus is excited by wavelengths from 400 nm to about 550 nm.
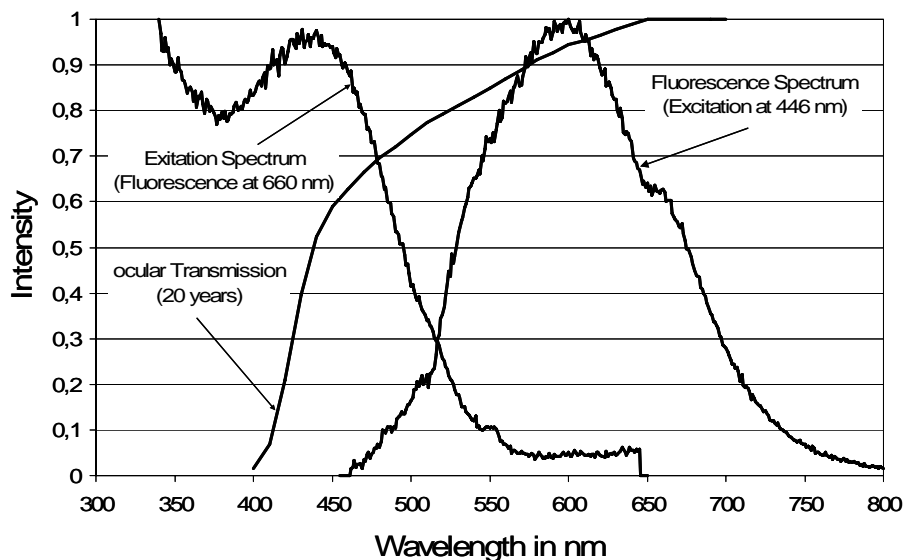

Fig. 1: Excitation and emission spectra of A2E, component VIII of Lipofuscin.

Excitation and emission spectra of the oxidised fluorescent form FAD of the redox pair FAD-FADH2 are shown in Fig. 2. For detection at 524 nm there are excitation maxima at 370 nm and 446 nm. Excitation at 446 nm or 470 nm results in fluorescence spectra having a single maximum at 524 nm. A comparison of the excitation spectrum with the transmission of the ocular media shows that also FAD is excited at the fundus.
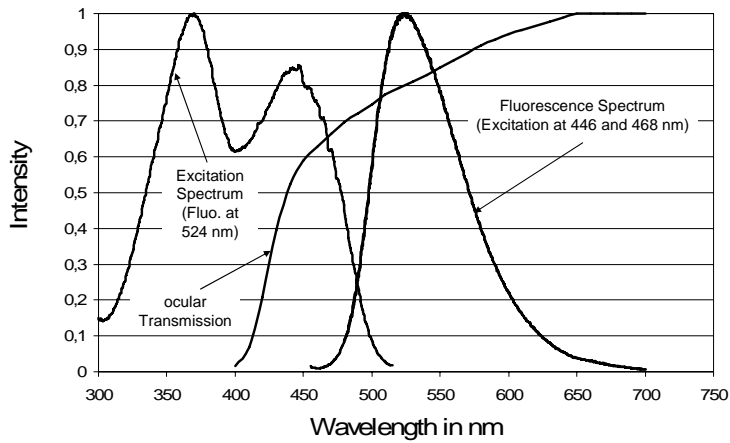
Fig. 2: Excitation and emission spectra of FAD

The excitation and emission spectra of NADH are shown in Fig. 3. For detection at 470 nm the excitation spectrum of NADH is broad and has a maximum at 340 nm. The excitation efficiency for wavelengths > 400 nm is so small that noticeable excitation of NADH at the fundus appears unlikely.

Very weak fluorescence spectra were detected for 446 nm and 470 nm excitation. The spectra have maxima at 514 nm and 528 nm, respectively. The fluorescence maximum of NADH is known to be at 450 nm (Cordeiro et al., 1995; Kobayashi et al., 2002; Tsubota et al., 1989). The fluorescence signals detected are therefore likely to originate from contamination.
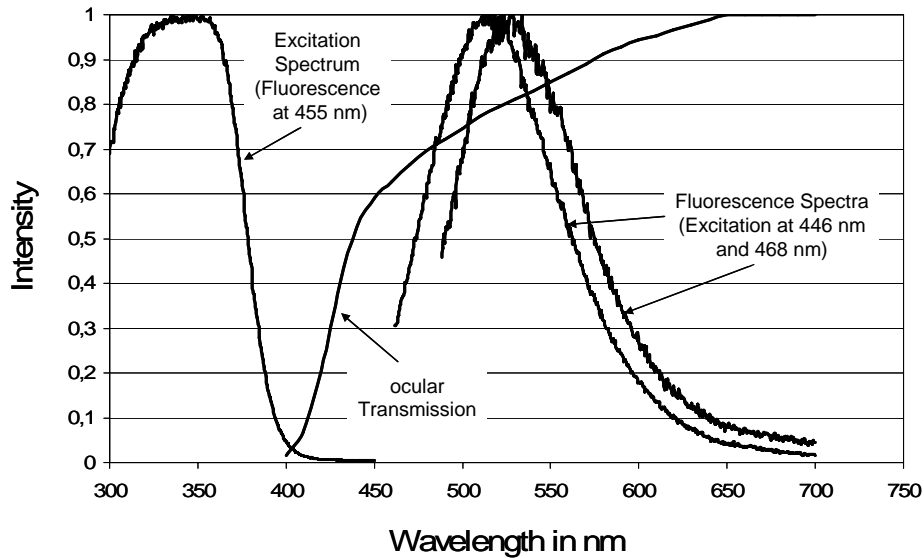
Fig. 3: Excitation spectrum of NADH. Excitation at 350 nm results in fluorescence maxima at 470 nm, but the fluorescence maxima at 514 nm and 524 nm after excitation at 446 nm and 468 nm originating probably from contamination

Excitation and emission spectra of advanced glycation end-products (AGE) are given in Fig. 4. Accumulation of AGE is a result of metabolic alterations, especially of diabetes mellitus. AGE is a mixture of different fluorophores. For fluorescence detection at 500 nm the excitation maximum is at 370 nm. Due to a wide shoulder at the long-wavelength end of the excitation spectrum AGE is substantially excited above 400 nm. For excitation at 446 nm and 470 nm the emission maximum is at 502 nm to 523 nm, respectively.
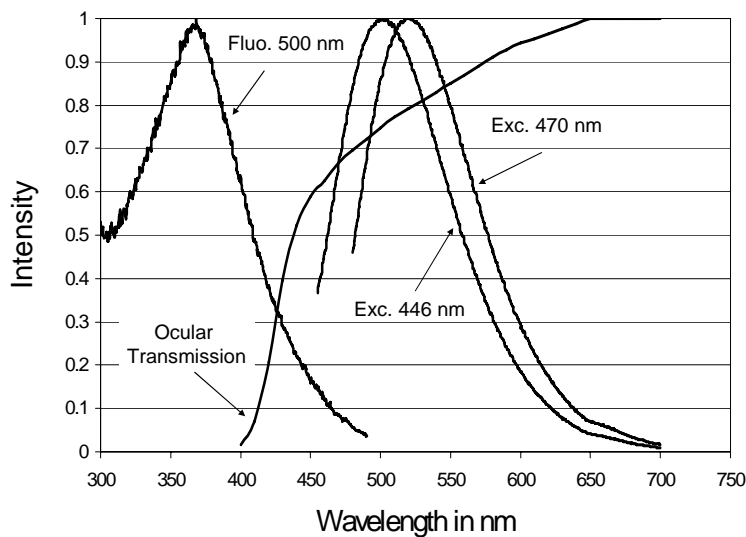

Fig. 4: Excitation and emission spectra of advanced glycation end-products (AGE)

In case of sclerotic processes an accumulation of connective tissue in the retina is expected. Fig. 5 shows the absorbance spectra of collagens and of elastin. The absorption maximum for collagens 1-4 and elastin is below 300 nm, but the spectrum is very broad. Especially for collagen 2 excitation at wavelengths > 400 nm is possible. There is little difference in the fluorescence spectra of collagen and elastin. When excited at 400 nm both have emission maxima between 460 nm and 470 nm.
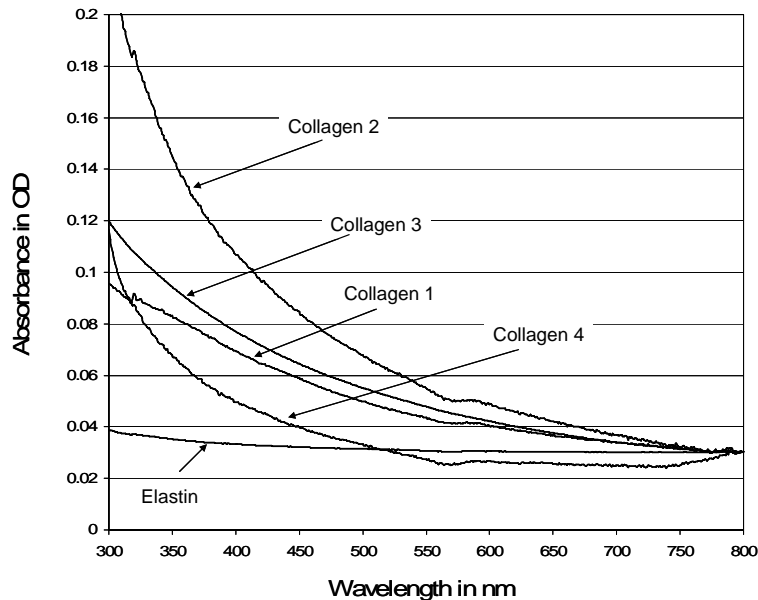

Fig. 5: Absorbance spectra of components of connective tissue (Collagen 1-4, Elastin).

Fig. 6 shows fluorescence spectra of collagen 2 for different wavelengths. Both a drop in efficiency and a shift of the emission maximum with increasing excitation wavelength was found. For excitation wavelengths of 400 nm, 446 nm, and 470 nm the emission maximum was found at 460 nm, 508 nm and 522 nm, respectively. Although the fluorescence intensity drops to 20% for excitation at 446 nm or 470 nm compared to excitation at 400 nm some contribution of connective tissue to the fundus fluorescence is likely.
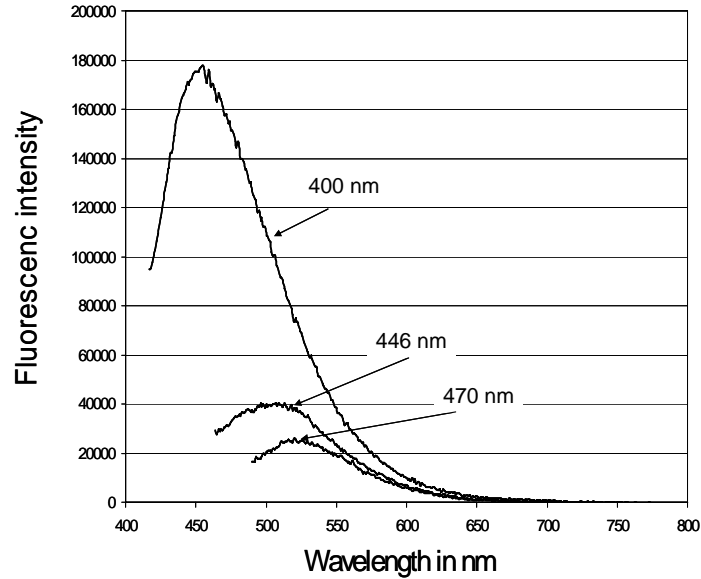
Fig. 6: Dependence of fluorescence intensity of Collagen 2 on excitation wavelength.

The colour of the fundus is determined by the absorption of melanin. This pigment is located in the choroid and in the retinal pigment epithelium. Retinal pigment epithelium is highly metabolic tissue. In this layer the discs of the outer receptor segment are continuously phagocytised. For detection 436 nm, the excitation maximum of melanin is at 360 nm. Extrapolating the excitation spectrum to wavelengths above 400 nm we do not expect a substantial contribution of melanin to the fundus fluorescence.
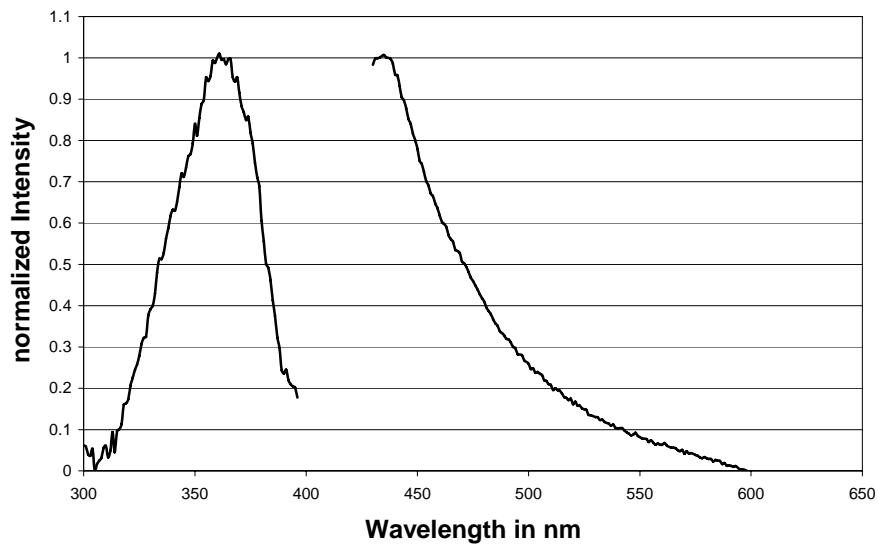

Fig. 7: Excitation and emission spectra of human ocular melanin. Excitation maximum at 360 nm, fluorescence maximum at 436 nm.

Fig. 8 shows effective excitation spectra of A2E, FAD, and of AGE. The spectra were calculated by taking into account the spectral transmission of the ocular media. The maxima of the effective

excitation spectra of A2E, FAD, and of AGE were found between 440 nm and 450 nm. At 450 nm all the fluorophores are excited. At longer excitation wavelength A2E dominates; above 500 nm almost exclusively A2E is excited. Thus, some discrimination of the fundus fluorophores can be obtained by varying the excitation wavelength.
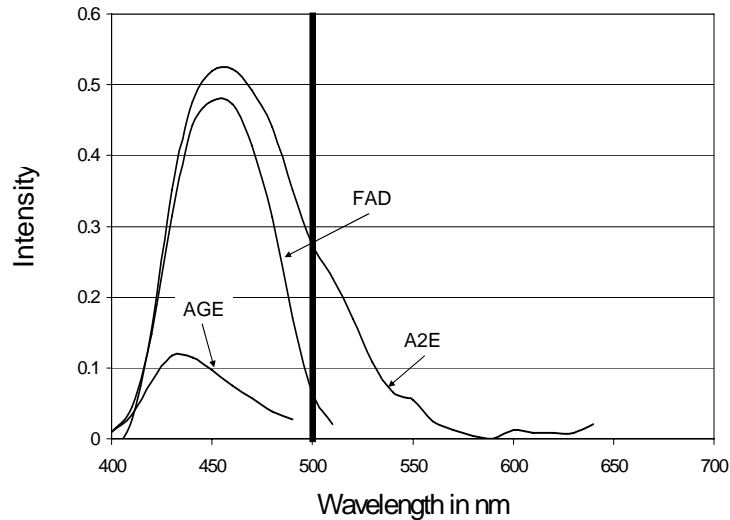
Fig. 8: Effective excitation spectra of A2E, FAD, and AGE

To further improve the discrimination of fluorophores, also the spectral range of fluorescence detection may be varied. Fig. 9 shows the normalised emission spectra of A2E, AGE, and FAD for excitation at 446 nm. The fluorescence in the range between 500 nm and 560 nm is dominated by FAD and AGE; the fluorescence above 560 nm is dominated by A2E and other components of Lipofuscin.
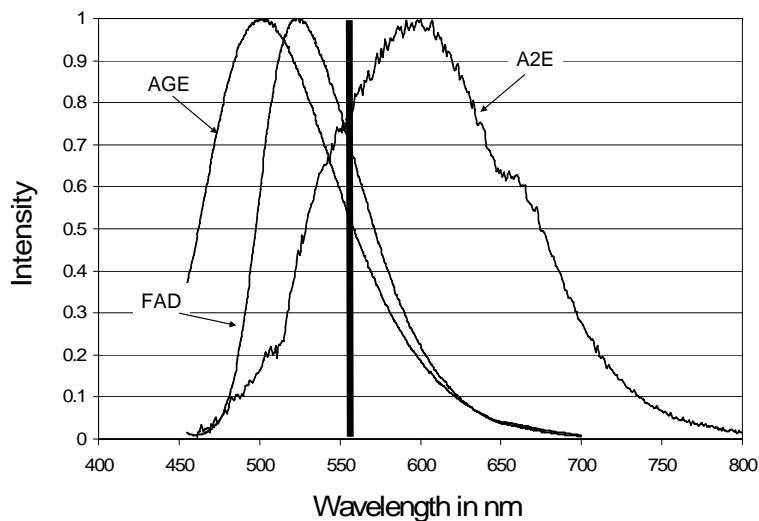
Fig. 9: Selected emission ranges for discrimination of fundus fluorophores.

Fluorescence Lifetimes of expected fundus fluorophores and of ocular tissue

In addition to excitation and emission spectra, fluorophores can be distinguished by their fluorescence lifetimes. Fluorescence decay curves of isolated endogenous fluorophores were recorded by TCSPC. The decay curves were fitted by a double-exponential model. The fit delivers two lifetime components, $\tau 1$ and $\tau 1$, and the corresponding amplitudes, a1 and a2. The results are shown in Table 1. For comparison, lifetimes and amplitudes are given also for ocular tissue, isolated from porcine eyes.

Substance	$\tau 1$ in ps	a1 in %	$\tau 2$ in ps	a2 in %
Collagen 1	670	68	4040	32
Collagen 2	470	64	3150	36
Collagen 3	345	69	2800	31
Collagen 4	740	70	3670	30
Elastin	380	72	3590	28
A2E	170	98	1120	2
Lipofuscin	390	48	2240	52
Melanin	280	70	2400	30
FAD	330	18	2810	82
AGE	865	62	4170	28
NADH	387	73	3650	27
Ocular tissue				
Retina	260	90	2790	10
RPE	210	96	1800	4
Choroid	500	70	3400	30
Sclera	450	65	3110	35
Cornea	570	70	3760	30
Lens	490	69	3600	31

Table 1: Fluorescence decay times of expected fundus substances and of porcine ocular tissues (Excitation at 446 nm, Emission range 510 nm to 700 nm, double-exponential approximation).

OPTIMISED SETUP FOR IN VIVO FLUORESCENCE LIFETIME IMAGING

The application of autofluorescence measurements as a diagnostic tool requires the discrimination of fluorophores in images of the ocular fundus. The differences in excitation and emission spectra can be used to optimise of the experimental setup for fluorescence lifetime imaging. Our setup is shown in Fig. 10. A picosecond diode laser (LDH 440 or LDH 470, Picoquant, Berlin, Germany) excites the fundus via a laser scanner ophthalmoscope (cSLO, Carl Zeiss, Oberkochen, Germany). The pulse width is about 100 ps (FWHM), the repetition rate 40 MHz. The fundus fluorescence is fed back through the scanner and split into two spectral components by a dichroic mirror, DM2. The wavelength intervals are 500 nm to 560 nm and 560 nm to 700 nm. Scattered excitation light is suppressed by a long pass filter, LP. The two signals are detected by two R3809U-50 MCP-PMTs (Hamamatsu).

The lifetime images are recorded by SPC-730, SPC-830, SPC-140 and SPC-150 TCSPC modules (Becker & Hickl, Berlin, Germany). These modules use a multi-dimensional TCSPC technique. For each individual photon, the location of the laser beam in the scanning area and the time in the fluorescence decay is determined and used to build up a photon distribution over the scanning area and the time. Thus, the technique is compatible with the fast scanning rate of the ophthalmic scanners. Moreover, the technique features multi-wavelength detection and excitation wavelength multiplexing capability. With an electrical time resolution of 6 ps (FWHM) and a time-channel width as small as 820 fs the signals are adequately sampled to satisfy the Nyquist criterion. Thus, fast components of double and triple-exponential decay profiles can be resolved. The multi-dimensional TCSPC technique is described in detail in (Becker, 2005).

The lifetime images of the autofluorescence were recorded for 40 degree fundus images. The pixel size was 80 x 80 μm^2. To obtain clear fundus images at this resolution the setup has to compensate for eye motion. After a saccade, the eye is in rest only for about 200 ms. Thus, a series of lifetime images of similarly short acquisition time is taken. The individual images are then aligned and accumulated. However, the individual fluorescence images do not contain enough photons to derive useful alignment vectors. Therefore we record reflection images at the excitation wavelength simultaneously with the fluorescence images. The reflected light is separated from the fluorescence light by a dichroic mirror, DM 1 (see Fig. 10).

The TCSPC images within the series were aligned and accumulated by an automatic affine transformation algorithm (Heidelberg Engineering, Heidelberg, Germany). Blurred imaged are recognised during the alignment procedure and automatically discarded.

The acquisition time depends on the number of decay components to be resolved, and on the desired lifetime accuracy. Currently the acquisition time for triple-exponential approximation of autofluorescence is about 10 minutes. The long acquisition time is due to the low photon count rate we obtain through our scanner optics. The count rates are about two orders of magnitude below the maximum count rate of the TCSPC technique used. We therefore expect that the acquisition time can be reduced by using a scanner of higher optical efficiency.
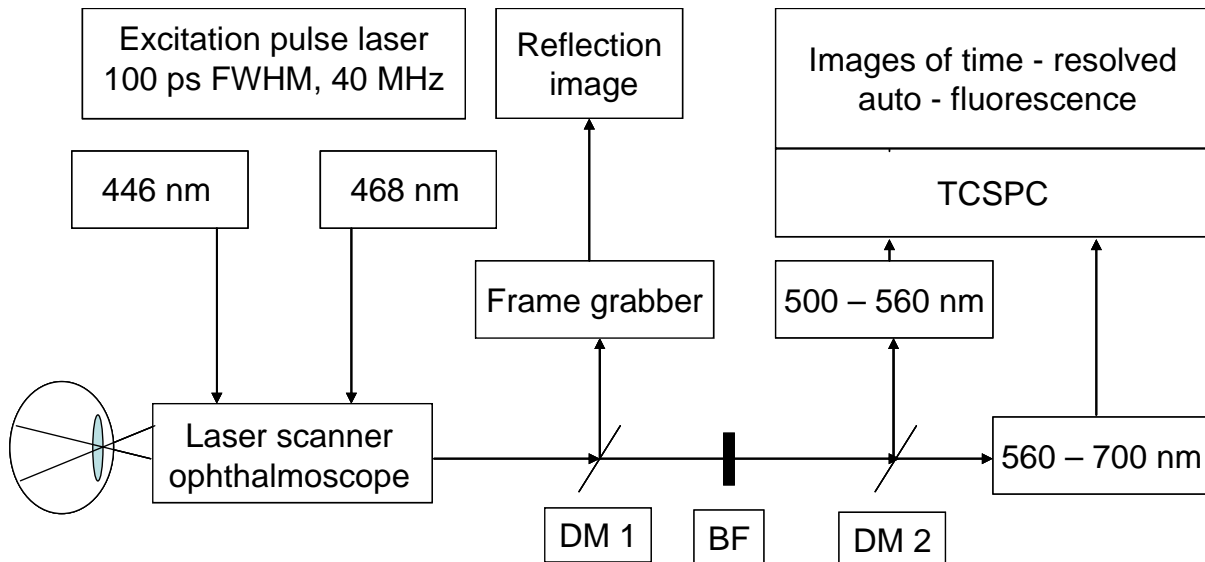

Fig. 10: Setup for fluorescence lifetime imaging of the human ocular fundus for excitation at different wavelengths and fluorescence detection in different spectral ranges.

The control menu of our 'EyeScan' recording system is shown in Fig. 11. The reflectance images are shown left. The reflectance image is used to adjust the ophthalmoscope before a measurement is started. An image of the fluorescence intensity is shown in the middle. It is obtained by accumulating the photons of all time channels in the individual pixels of the TCSPC FLIM data. A fluorescence decay curve at a selected pixel is shown right. FLIM data analysis was performed by using the SPCImage 2.7 software (Becker & Hickl, Berlin). For each pixel the decay data were fitted by a triple-exponentially decay model (Lakowicz, 1999). As a result of the fit procedure, images can be represented by three lifetimes, $\tau 1$, $\tau 2$, and $\tau 3$, and three amplitudes, a1, a2, and a3, or relative integral intensities, Q1, Q2, and Q3, see Fig. 12 (Schweitzer et al., 2004b). For typical images, the number of photons in the individual pixels is on the order of 10,000. It should be mentioned here that the calculation of reasonable triple-exponential decay parameters from only 10,000 photons is in apparent disagreement with Köllner and Wolfrum (Köllner and Wolfrum, 1992) who estimated that a number of 400,000 photons would be needed to resolve a double-exponential decay consisting of 10% of 2 ns and 90% of 4 ns. Fortunately, in the present case the lifetime components are much wider apart, and the amplitude of the fastest component is large. This makes the analysis considerably easier.

The images of the decay parameters allow the user to interpret the dynamic behaviour of the fundus autofluorescence. Moreover, images of reduced χ^2 give an impression of the quality of the fit at all fundus sites. A more objective interpretation of the data can be achieved with 'scatter plots', i.e. diagrams showing $\tau 3$ or $\tau 2$ values versus $\tau 1$ values for the individual pixels (Schweitzer et al., 2004b; Schweitzer et al., 2005b). Based on these diagrams cluster plots for isolated fluorophores, ocular tissue or of selected ranges of the fundus can be obtained. These allow the user, to a certain degree, to derive a substance-specific interpretation of in vivo lifetime measurements. A further step in metabolic functional diagnostics may be based on local values of Q1, Q2, and Q3 in of images of dynamic fluorescence. In such diagrams, local differences can be discovered in the fluorescence contribution of single layers.
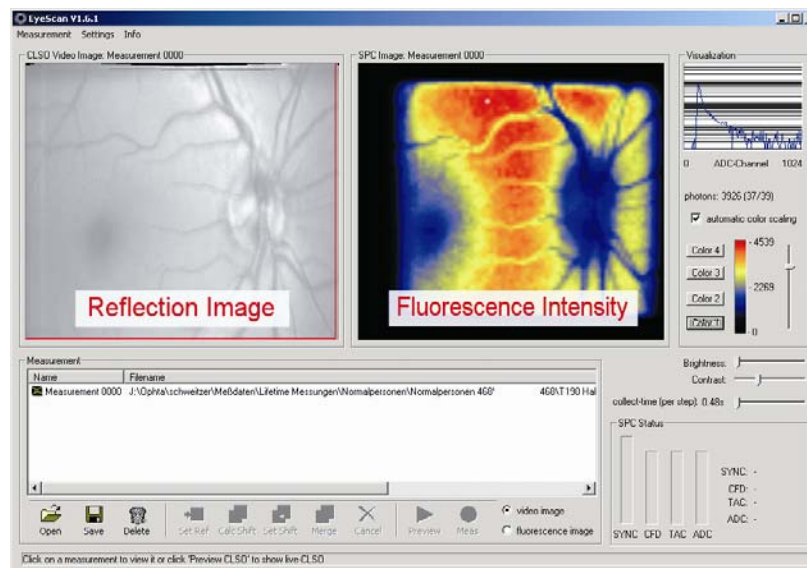

Fig. 11: Control menu 'EyeScan' of the lifetime mapper. Left: Reflectance image. Middle: fluorescence intensity image. Upper right: Decay function in a selected spot.

RESULTS

Lifetime images in the spectral range from510 nm to 700 nm

Fig. 12 shows the analysed data measured at a 25 year old healthy volunteer. The excitation wavelength was 468 nm. A long-pass filter of 510 nm transition wavelengths (HQ510 LP, LOT, Darmstadt, Germany) was used in the detection path. No further separation of emission ranges was performed. The image of the fluorescence intensity is shown left. A lifetime image of the shortest lifetime component, $\tau 1$, is shown in the middle. The lifetime is presented by the colour; red to blue corresponds to 100 to 300 ps. Both macula and optic disc appear dark in fluorescence intensity images. Nevertheless, clearly different lifetimes, $\tau 1$, are obtained for these structures. The smalles values of $\tau 1$ were detected in the macular range ($\tau 1$ about 150 ps); the largest values in the optic disc ($\tau 1 > 250$ ps). The most frequent value of $\tau 1$ was around 190 ps. A corresponding histogram of $\tau 1$ is presented in the right part of the SPCImage panel. In the lower part of Fig. 12 the decay curve at the selected position, the residual of the fit, and the lifetimes and amplitudes of the decay components are displayed. The model accounts also for a possible shift between the fluorescence decay and the instrumental response, scattered excitation light, and continuous background by ambient light or detector dark counts.
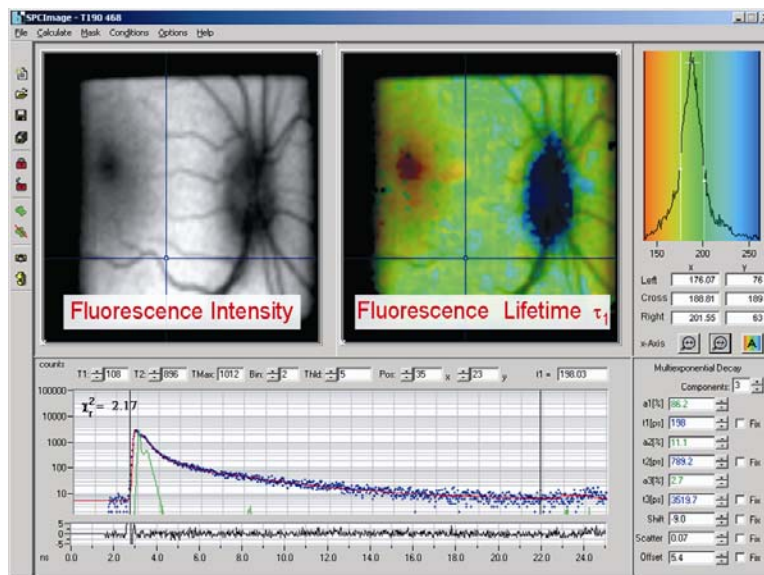

Fig. 12: SPCImage-menu for calculation of lifetimes. Left: image of fluorescence intensity, middle: image of lifetime $\tau 1$, right: histogram of $\tau 1$, below: left measured photon distribution, instrumental response, and model function, right: amplitudes and lifetimes of a selected pixel, bottom: curve of residuals

A fluorescence lifetime image of a patient suffering from geographic atrophy is shown in Fig. 13. This patient had an implanted artificial intra-ocular lens. The fluorescence was excited at 446 nm. In this case, a double-exponential approximation was sufficient to fit the decay profiles. The fast lifetime component, $\tau 1$, in the macula is as long as in the optic disc, indicating an increased contribution of fluorescence of connective tissue.
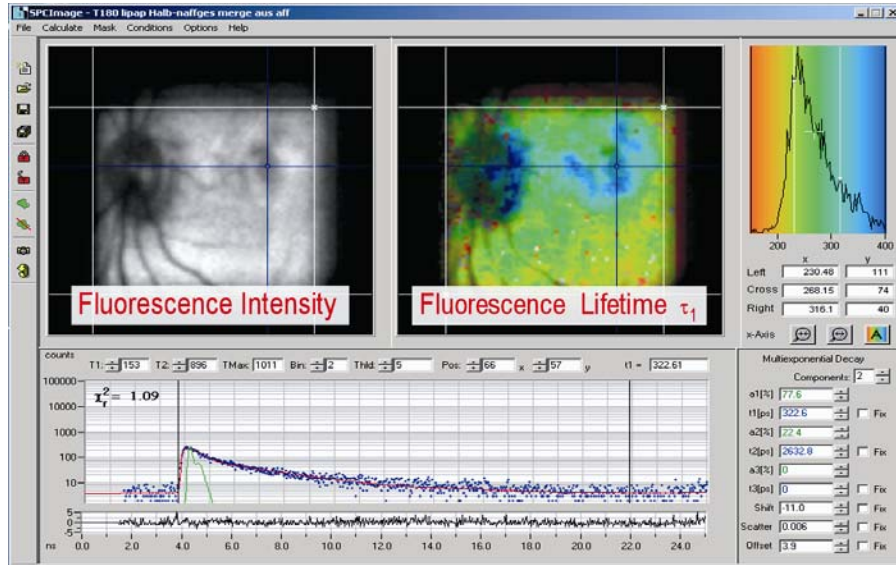
Fig. 13: Fluorescence lifetime image of a patient suffering from geographic atrophy.

Histograms of lifetime components for different excitation wavelength

The effect of different excitation wavelengths is demonstrated in Fig. 14. The diagrams show histograms of the frequency of pixels with a given value of the fast lifetime component, $\tau 1$, of a triple-exponential decay model. The histograms are shown for excitation at 446 nm (left) and 468 nm (right). As expected from the effective excitation spectra (Fig. 8) excitation at 446 nm results in the excitation of several fluorophores and thus in a wider distribution than excitation at 468 nm. This effect is most clearly seen in the histograms of $\tau 1$. For excitation at 446 nm maxima in the histogram of $\tau 1$ are found at 100 ps, 120 ps, 165 ps, 185 ps, and 220 ps. In contrast, excitation at 468 nm results in a single dominating lifetime component of $\tau 1 = 190\pm10$ ps. Furthermore, excitation at 446 nm results in maxima for $\tau 2$ at 1100 and 1350 ps, and 5000 ps for $\tau 3$. Excitation at 468 nm results in a single maximum for $\tau 2$ at 750±50 ps and for $\tau 3$ at 3550±200 ps.
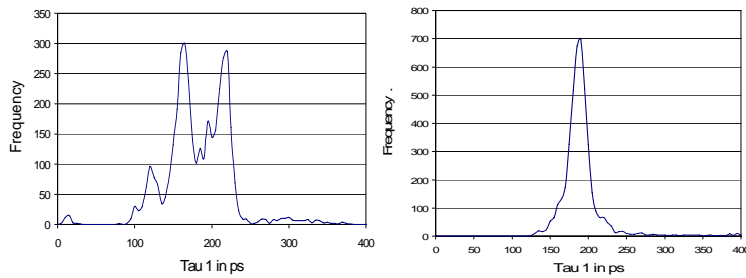

Fig. 14: Histograms of lifetime $\tau 1$ for excitation at 446 nm (left) and 468 nm (right) as result of triple-exponential approximation of 40 degree fundus autofluorescence images of a healthy person.

Detection of fluorescence in different spectral ranges

The expected influence of different fluorophores in selected emission wavelength ranges (Fig. 9) was verified by measurements at the fundus of a healthy volunteer.

Fig. 15, left and right, shows fluorescence images detected in wavelength intervals of 510 nm to 560 nm and 560 nm to 700 nm, respectively. The excitation wavelength was 468 nm. In the left (510 nm to 560 nm) image the retinal vessels have low contrast while they are clearly visible in the right (560 nm to 700 nm) image. That means, the fluorophore emitting at 560 nm to 700 nm is located behind the vessel system. In this wavelength range the fluorescence is dominated by lipofuscin. Lipofuscin is mainly located in the retinal pigment epithelium (RPE), i.e. behind the blood vessels. The reduced contrast in the 510 nm to 560 nm image is caused by the autofluorescence of fundus layers in front of the RPE.
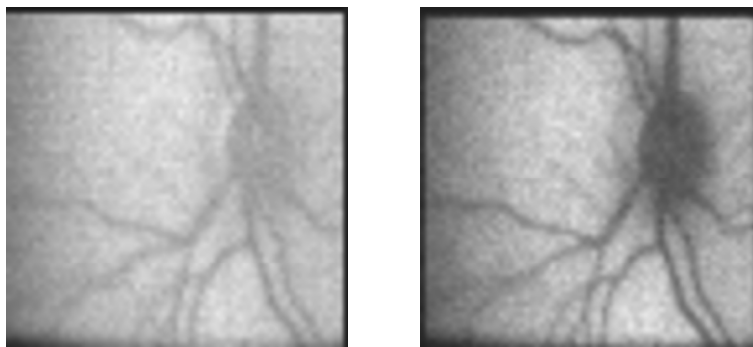

Fig. 15: Images of fluorescence intensity excited at 468 nm and detected between 510 nm and 560 nm (left) as well as between 560 nm and 700 nm (right)

Fig. 16 shows a histological section of a porcine fundus. It is likely that a large part of the fluorescence at 510 nm to 560 nm comes from receptors or ganglion cells .
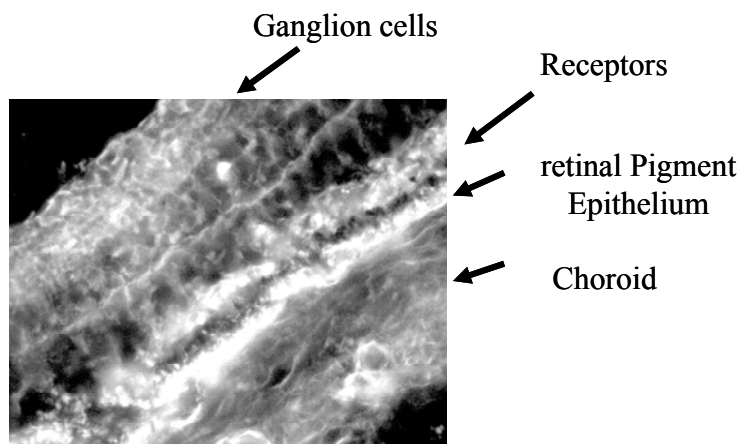

Fig. 16: Autofluorescence of a histological section of a porcine fundus. Excitation range 450 nm to 490 nm, emission > 520 nm.

Relationship between components of triple-exponential approximation and anatomical structures

Information about the origin of the relative intensity contributions of the three lifetime components, Q1, Q2, and Q3, to the ocular fluorescence was derived from their spatial distribution. The component Q1 was found to be negligible in the optic disc. Thus, Q1 can be assigned to the RPE which is known to be absent within the optic disc. Q3 was found at maximum in the optic disc, while Q2 was uniformly distributed. Taken into account ex vivo measurements in porcine eyes, this finding suggests that Q2 is linked to the neural retina and Q3 to the connective tissue and, to a certain degree, to the fluorescence of the crystalline lens. The influence of the lens is supported by different values of $\tau 3$ found in healthy subjects and patients wearing intra-ocular lenses.

Fig. 17 shows the relative contributions of the three lifetime components for sections across the macula of a patient with early AMD (left) and late AMD (right). The differences in the contribution profiles may be indicative of age-related macular degeneration.
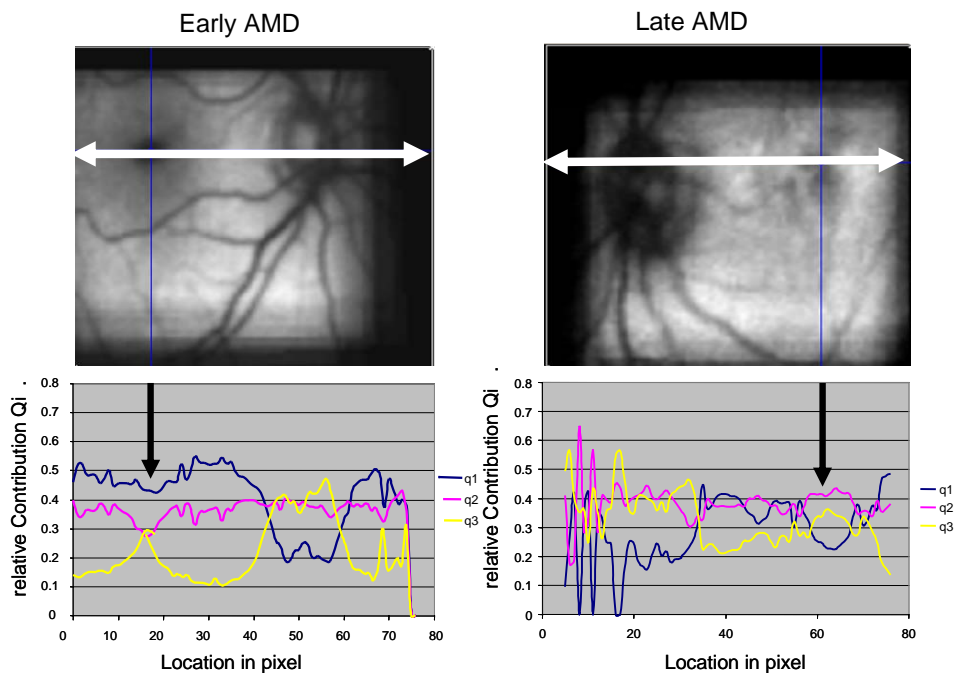

Fig. 17: Macular sections of relative intensity contributions of the lifetime components, Qi, of a triple-exponential fit.

Conclusions

Metabolic alterations in the retina result in changes in the contribution of individual fluorophores to the total fluorescence or in the appearance of new fluorescence components. Detecting such alterations are helpful to the diagnosis of early stages of age-related macular degeneration. However, due to the spectral transmission characteristics of the ocular media the choice of excitation and detection wavelengths is very limited. The excitation of NADH appears unlikely. The fluorescence of lipofuscin, FAD, AGE, and collagen is detectable from the fundus. Weak

fluorescence signals may be also obtained from melanin. A limited separation of the fluorescence components by optimising the excitation and detection wavelengths is possible, but a complete separation of all contributing fluorophores does not appear feasible.

The prospects of detecting metabolic alterations are better for fluorescence lifetime detection. The fluorescence lifetime is not influenced by the wavelength-dependent transmission of the ocular media or by the spectral absorption of substances weakening the fluorescence light. Fluorescence lifetime images of the fundus recorded by TCSPC FLIM were analysed by a triple-exponential decay model. The analysis yields three lifetime components, the corresponding amplitudes, and the relative intensity contributions for all pixels of the image. These data, in turn, were used to build up histograms of the frequency of different values of the lifetime components in the pixels of an image area. The lifetime components could thus be attributed to different fluorescing species and anatomic structures.

The lifetime histogram of the fast decay component, $\tau 1$, has several maxima for excitation at 446 nm. For excitation at 468 nm only a single maximum is obtained. Taking into account the effective excitation and emission spectra, we conclude that predominately A2E and other components of lipofuscin are excited at 468 nm.

A comparison of fluorescence images taken at different emission wavelength with images of histological sections indicate that the fast decay component, with a lifetime of about 190 ps and an amplitude of about 90 %, is related to the retinal pigment epithelium. The second fastest component, of about 1 ns lifetime and about 10 % amplitude, seems to be related to the neural retina. A third decay component, with a lifetime of 3.5 ns, originates in the crystalline lens and the connective tissue.

We found differences in the intensity contributions of the three lifetime components for healthy persons, patients with early AMD, and patients with late AMD. We therefore believe that fluorescence lifetime imaging of the fundus is more indicative of AMD than intensity imaging at selected excitation and emission wavelengths.

REFERENCES

ANSI (2000) *American National Standard for the safe use of laser. ANSI Z 136.1-2000*. Orlando, Suite 128, 13501 Ingenuite Drive, FL 32826, Laser Institute of America.

Beach JM, Schwenzer KJ, Srinivas S, Kim D, Tiedeman JS. 1999. Oximetry of retinal vessels by dual-wavelength imaging: calibration and influence of pigmentation. J Appl Physiol **86**(2), 748-58.

Becker W. 2005. *Advanced time-correlated single photon counting technique.* Berlin, Heidelberg, New York: Springer.

Bindewald A, Bird AC, Dandekar SS, Dolar-Szczasny J, Dreyhaupt J, Fitzke FW, Einbock W, Holz FG, Jorzik JJ, Keilhauer C, Lois N, Mlynski J, Pauleikhoff D, Staurenghi G, Wolf S. 2005. Classification of fundus autofluorescence patterns in early age-related macular disease. Invest Ophthalmol Vis Sci **46**(9), 3309-14.

Bird DK, Yan L, Vrotsos KM, Eliceiri KE, Vaughan EM. 2005. Metabolic mapping of MCF10A human brest cells via multiphoton fluorescence lifetime imaging of coenzym NADH. Cancer Res **65**(19), 8766-8773.

Chance B. 1976. Pyridine nucleotide as an indicator of the oxygen requirements for energy-linked functions of mitochondria. Circ-Res. **38**(5 Suppl 1), I 31-I 38.

Cordeiro PG, Kirschner RE, Hu QY, Chiao JJ, Savage H, Alfano RR, Hoffman LA, Hidalgo DA. 1995. Untraviolet excitation fluorescence spectroscopy: a noninvasive method for the measurement of redox changes in ischemic myocutaneous flaps. Plast Reconstr Surg **96**(3), 673-680.

Cunha-Vaz JG, Lima JP. 1978. Studies on retinal blood flow. I. Estimation of human retinal blood flow by Slit-lamp fluorophotometry. Arch Ophthalmol **29**, 893-897.

Delori FC, Dorey KC, Staurenghi G, Arend O, Goger DC, Weiter JJ. 1995. In vivo fluorescence of the ocular fundus exhibits retinal pigment epithelium lipofuscin characteristics. Invest. Ophthalmol. **36**, 718-729.

Delori FC, Goger DG, Hammond BR, Snodderly DM, Burns SA. 2001. Macular pigment density measured by autofluorescence spectrometry: comparison with reflectometry and heterochromatic flicker photometry. J. Opt. Soc. Am. A **18**(6), 1212-1229.

Delori FC, Parker JS, Mainster MA. 1981. Retinal vessel oximetry. In *ARVO Meeting Sarasota 27.4.-1.5.1981*.

Einbock W, Moessner A, Schnurrbusch UE, Holz FG, Wolf S. 2005. Changes in fundus autofluorescence in patients with age-related maculopathy. Correlation to visual function: a prospective study. Graefes Arch Clin Exp Ophthalmol **243**(4), 300-5.

Eldred GE, Katz ML. 1988. Fluorophores of the human retinal pigment epithelium: Separation and spectral characterization. Exp. Eye Res. **47**, 71-86.

Eldred GE, Lasky MR. 1993. Retinal age-pigments generated by self-assembling lysosomotropic detergents. Nature **361**, 724-726.

Feeney-Burns L, Berman ER, Rothman H. 1980. Lipofuscin of human retinal pigment epithelium. Am J Ophthalmol **90**(6), 783-91.

Geeraets WJ, Berry ER. 1968. Ocular spectral characteristics as related to hazards from lasers and other light sources. Am Jour. Ophthal. **66**(1), 15-20.

Gerritsen HC, Asselbergs MAH, Agronskaia AV, van Sark WGJHM. 2002. Fluorescence lifetime imaging in scanning microscopes: acquisition speed, photon economy and lifetime resolution. J. Microsc. **206**, 218-224

Hickham JB, Frayser R, Ross JC. 1963. A study of retinal venous blood oxygen saturation in human subjects by photographic means. Circulation **27**, 375-385.

Holz FG, Bellman C, Staudt S, Schuett F, Volcker HE. 2001. Fundus autofluorescence and development of geographic atrophy in age- related macular degeneration. Invest Ophthalmol Vis Sci **42**(5), 1051-6.

Ishibashi T, Murata T, Hanagai M, Nagai R, Horiuchi S, Lopez PF, Hinton DR, Ryan SJ. 1998. Advanced glycation end products in age related macular degeneration. Arch. Ophthalmol. **116**(12), 1629-1632.

Kobayashi M, Shibuya K, Hoshino H, Fujisawa T. 2002. Spectroscopic analysis of autofluorescence from human bronchus using an ultraviolet laser diode. J Biomed Opt. **7**(4), 603-608.

Köllner M, Wolfrum J. 1992. How many photons are necessary for fluorescence-lifetime measurements? Phys. Chem. Lett. **200**, 199-204

Laing RA, Danisch LA, Young LR. 1975. The Choroidal Eye Oximeter: An Instrument for Measuring Oxygen Saturation of Choroidal Blood In Vivo. IEEE Transaction on Biomedical Engineering **22**, 183-195.

Lakowicz JR. 1999. *Principles of Fluorescence Spectroscopy*. New York, Boston, Dondrecht, London, Moscow: Kluwer Academic/Plenum Publishers.

Oswald B, Vilser W, Oswald H, Jütte A, Königsdörffer E, Schweitzer D. 1983. Messung von strömungsphysiologischen Größen der Netzhautdurchblutung bei Normalpersonen. Graefe´s Arch Clin Exp Ophthalmol **220**, 39-41.

Parish CA, Hashimoto M, Nakanishi K, Dillon J, Sparrow J. 1998. Isolation and one step preparation of A2E and iso-A2E, fluorophores from human retinal pigment epithelium. Proc. Natl. Acad. Sci. USA **95** (Biochemistry), 14609-14613.

Pokorny J, Smith VC, Lutze M. 1987. Aging of the human lens. Appl. Opt. **26**, 1437-1440.

Qui L, Zhao W, Sick T. 2005. Quantitative analysis of brain NADH in the presence of hemoglobin using microfiber spectrofluorometry: a pre-calibration approach. Comput Biol Med **35**(7), 583-601.

Riva CE, Ross B, Benedek GB. 1972. Laser Doppler measurements of blood flow in capillary tubes and retinal arteries. Invest. Ophthalmol **11**, 936-944.

Sato E, Feke GT, Menke MN, Wallace McMeel J. 2006. Retinal haemodynamics in patients with age-related macular degeneration. Eye **20**(6), 697-702.

Schweitzer D, Hammer M, Anders R, Doebbecke T, Schenke S. 2004a. Veränderungen der Autofluoreszenzlebensdauer am Fundus nach Sauerstoffprovokation. Ophthalmologe **101**(1), 66-72.

Schweitzer D, Hammer M, Kraft J, Thamm E, Königsdörffer E, Strobel J. 1999. In Vivo Measurement of the Oxygen Saturation of Retinal Vessels in Healthy Volonteers. IEEE Trans. Biomed. Eng. **46**, 1454-1465.

Schweitzer D, Hammer M, Schweitzer F. 2005a. Grenzen der konfokalen Laser Scanning Technik bei Messungen der zeitaufgelösten Autofluoreszenz am Augenhintergrund. Biomed. Technik **50**(9), 263-267.

Schweitzer D, Hammer M, Schweitzer F, Anders R, Doebbecke T, Schenke S, Gaillard ER. 2004b. In vivo measurement of time - resolved autofluorescence at the human fundus. J. Biomed. Opt. **9**(6), 1214-1222.

Schweitzer D, Kolb A, Hammer M, Thamm E. 2000. Tau-mapping of the autofluorescence of the human ocular fundus. Proceedings of SPIE **4164**, 79-89.

Schweitzer D, Leistritz L, Hammer M, Scibor M, Bartsch U, Strobel J. 1995. Calibration-free measurement of the oxygen saturation in retinal vessels of men. In *Proc . of the "Symposon on Biomedical Optics 1995"*, pp. 210-218. San Jose: Proc. SPIE.

Schweitzer D, Schweitzer F, Hammer M, Schenke S, Richter S. 2005b. Comparison of time-resolved autofluorescencein the eye-ground of healthy subjects and patients suffering from age-related macular degeneration. Progress in Biomedical Optics and Imaging **6**(31), 58625R-1 - 58620R-12.

Sparrow JR, Fishkin N, Zhou J, Cai B, Jang YP, Krane S, Itagaki Y, Nakanishi K. 2003. A2E, a byproduct of the visual cycle. Vision Res **43**(28), 2983-90.

Sparrow JR, Nakanishi K, Parrish CA. 2000. The lipofuscin fluorophore A2E mediates blue light-induced damage to retinal pigment epithelial cells. Invest Ophthalmol Vis Sci **41**, 1981-1989.

Tsubota K, Krauss JM, Kenon KR, Laing RA, Miglior S, Cheng HM. 1989. Lens redox fluorometry: pyridine nucleotide fluorescence and analysis of diabetic lens. Exp Eye Res. **49**(3), 321-334.

van Norren D, Vos JJ. 1974. Spectral transmission of the human ocular media. Vision Res. **14**, 1237-1244.

Vilser W, Juette A, Seewald D, Dietze U, Friedrich R, Koenigsdoerffer E, Buechner D. 1986. Measurement of retinal microcirculation in retinal vessel occlution before and after treatment. Graefes Arch Clin Exp Ophthalmol **224**(2), 179-183.

von Rückmann A, Fitzke FW, Bird AC. 1995. Distribution of fundus autofluorescence with a scanning laser ophthalmoscope. Brit. J. Ophthalmol **79**, 407-412.

von Rückmann A, Fitzke FW, Fan J, Halfyard A, Bird AC. 2002. Abnormalities of fundus autofluorescence in central serous retinopathy. Am. J. Ophthalmol. **133**(6), 780-786.